Available online at www.sciencedirect.com

ScienceDirect

Advances in Space Research 65 (2020) 2247–2262

ADVANCES IN SPACE RESEARCH (a COSPAR publication)

www.elsevier.com/locate/asr

Downsizing an orbital space robot: A dynamic system based evaluation

Lucy Jackson [a,*], Chakravarthini M. Saaj [b], Asma Seddaoui [a], Calem Whiting [c], Steve Eckersley [c], Simon Hadfield [a]

[a] Surrey Space Center, University of Surrey, GU2 7XH, UK
[b] University of Lincoln, LN6 7TS, UK
[c] Surrey Satellite Technology Ltd, Tycho House, GU2 7YE, UK

Received 24 June 2019; received in revised form 11 February 2020; accepted 7 March 2020
Available online 19 March 2020

Abstract

Small space robots have the potential to revolutionise space exploration by facilitating the on-orbit assembly of infrastructure, in shorter time scales, at reduced costs. Their commercial appeal will be further improved if such a system is also capable of performing on-orbit servicing missions, in line with the current drive to limit space debris and prolong the lifetime of satellites already in orbit. Whilst there have been a limited number of successful demonstrations of technologies capable of these on-orbit operations, the systems remain large and bespoke. The recent surge in small satellite technologies is changing the economics of space and in the near future, downsizing a space robot might become be a viable option with a host of benefits. This industry wide shift means some of the technologies for use with a downsized space robot, such as power and communication subsystems, now exist. However, there are still dynamic and control issues that need to be overcome before a downsized space robot can be capable of undertaking useful missions. This paper first outlines these issues, before analyzing the effect of downsizing a system on its operational capability. Therefore presenting the smallest controllable system such that the benefits of a small space robot can be achieved with current technologies. The sizing of the base spacecraft and manipulator are addressed here. The design presented consists of a 3 link, 6 degrees of freedom robotic manipulator mounted on a 12U form factor satellite. The feasibility of this 12U space robot was evaluated in simulation and the in-depth results presented here support the hypothesis that a small space robot is a viable solution for in-orbit operations.
© 2020 COSPAR. Published by Elsevier Ltd. This is an open access article under the CC BY license (http://creativecommons.org/licenses/by/4.0/).

Keywords: Small satellite; Space robot; In-orbit assembly and servicing; In-orbit operations; Free-flying; Free-floating

1. Introduction

There is an ever growing demand for autonomous robots in the space industry and intelligent space robots are likely to remain an integral part of space exploration. The use of robotic systems to carry out on-orbit operations is highly desirable, since it limits the need for astronaut intervention in extreme environments, meaning missions can be executed in shortened times scales, with higher levels of human safety. The first robotic system used in space was the Shuttle Remote Manipulator System (SRMS), which was deployed from the cargo bay of the Space Shuttle in 1981 and aided in the assembly of the International Space Station (ISS) (Flores-Abad et al., 2014). It was a 15.2 m long, robotic manipulator, with 6 degrees of freedom (DoF) (Rembala and Ower, 2009). Since then more bespoke robotic manipulators have been developed, the European Space Agency (ESA) have developed the European Robotic Arm (ERA) which is due to operate off the Russian segment of the ISS, and the Canadian Space

* Corresponding author.
E-mail addresses: l.jackson@surrey.ac.uk (L. Jackson), msaaj@lincoln.ac.uk (C.M. Saaj), a.seddaoui@surrey.ac.uk (A. Seddaoui), c.whiting@sstl.co.uk (C. Whiting), s.eckersley@sstl.co.uk (S. Eckersley), s.hadfield@surrey.ac.uk (S. Hadfield).

https://doi.org/10.1016/j.asr.2020.03.004
0273-1177/© 2020 COSPAR. Published by Elsevier Ltd.
This is an open access article under the CC BY license (http://creativecommons.org/licenses/by/4.0/).

Agency have reinvented the SRMS, now named the Space Station Remote Manipulator System (SSRMS) (Sallaberger, 1997). However, the large size of these robotic manipulators and base onto which they are mounted, means systems are all costly and bespoke, with long lead times. ESA first proposed the ERA in 1996, and as of 2019, it is yet to operate in situ (Boumans and Heemskerk, 1998). The size of the systems also impose constraints on the level of precision and flexibility allowable in mission and payload design. Large manipulators make the tightening of small interfaces or replacement or critical electrical components an unattainable task. The next step in unlocking the potential of space robots is therefore to reduce their size. The proposal of a small, free-flying, space robot capable of operating in orbit offers a simple low-cost alternative to the larger bespoke systems. Smaller systems will be capable of carrying out tasks currently beyond the capability of robotic systems already available. On top of this, smaller systems will take up less space in launch vehicle fairings, making them easier and cheaper to deploy relative to their heavier counterparts, further increasing their commercial appeal.

Free-flying robotic manipulators were introduced as a potential solution to the issues that these fixed robotic manipulators could not satisfy, and are not proposed as a replacement to the larger robotic arms. The first example of such a technology demonstration mission was in 1997, when the Experimental Test Satellite (EST-VII) launched. The manipulator had 6 DoF and a reach of 2 m; and was mounted on a 2.5 ton chaser satellite, that was able to rendezvous with a cooperative target spacecraft (Oda, 1999). This mission came to an end when time delays in the control system, meant the reaction forces, as a result of the dynamic coupling, could not be counteracted quickly enough, causing the system to become unstable (Penin et al., 2000). Improvements in control theory and sensing capability meant this was not an issue for Boeing and the Defense Agency Research Projects Agency (DARPA), who designed the Orbital Express mission. Launched in 2007, it was designed to validate the feasibility of rendezvous and autonomous refueling (Mulder, 2008). This mission proved much more successful than its precursor, although the hardware remained large, with the base spacecraft weighing in at 1 ton (Friend, 2008).

Following this, technology demonstrations of free-flying space robots capable of operating in-orbit remain in the conceptual stage. DLR developed the DEOS mission, which aimed to demonstrate the feasibility of maintenance and servicing, but never progressed beyond the preliminary design definition stage (Reintsema et al., 2011). Another program, named the Front-end Robotics Enabling Near-term Demonstration (FREND), designed to service satellites not built to enable robotic interaction was developed by DARPA (Debus and Dougherty, 2009). This technology has been fully tested at laboratory level but is yet to launch (Flores-Abad et al., 2014). This manipulator has been suggested for use in a range of servicing missions, including DARPA's PHOENIX mission, NASA's Restore-L mission and DARPA's RSGS mission (Nanjangud et al., 2018; Reed et al., 2016; Sullivan et al., 2015). NASA is also developing the Tendon-Actuate Lightweight In-Space MANipulator (TALISMAN) in house, which is designed for use exclusively with assembly missions (Doggett et al., 2014). This hardware is the cornerstone for NASA's latest project, known as the Commercial Infrastructure for Robotic Assembly and Services (CIRAS), which aims to demonstrate the ability of space-based robotic assembly by attaching and detaching solar arrays (Bowman et al., 2018; Roa et al., 2017). These technologies are considered large in the context of this study, however, with the FREND manipulator weighing 78 kg, and the TALISMAN manipulator weighing 36.2 kg, the commercial drive to provide a smaller space robot is becoming apparent (Debus and Dougherty, 2009; Doggett et al., 2014).

While none of these systems have launched, some small robotic systems have. RSat is a small space robot, equipped with 2 robotic manipulators mounted onto a 3U base spacecraft. It launched in 2018 and operates under 'constant hold' conditions (Wenberg et al., 2016; Wenberg et al., 2018). This means that it can traverse along a payload and perform tasks without ever losing contact. The base onto which the manipulators are mounted therefore has no control system and the dynamic coupling effect is not of concern. The Synchronized Position Hold Engage and Reorient Experimental Satellites (SPHERES), launched to the ISS in 2006, and demonstrated close flying and control algorithms in a micro-gravity operating environment. They have since demonstrated docking and rendezvous, as a result of a hardware upgrade (Chung et al., 2006). Further development of these satellites has led to a proposal that they be used for on-orbit operations; in conjunction with the Assembly of Large Modular Telescopes (ALMOST) mission. This combined program would involve dependent payload actuation through the use of a flexible tether, although its validity is yet to be tested (Miller et al., 2008). Dependent payload actuation is when a space robot can only actuate a payload by relocating the entire system, this occurs if it is equipped with a 0 DoF arm or flexible tether. The use of dependent payload actuation again means that the phenomenon of dynamic coupling is not a cause for concern. Both these systems demonstrate the commercial demand and technology readiness of the hardware required for such small robotic systems, including: sensing, communications, power generation and processing subsystems. However, neither have tackled the issue of the increased control demand due to the dynamic coupling effect. This is of particular concern in the case of small free-flying robots since the inertia of the arm is non-negligible in comparison to the base. This highlights the need for the dynamic analysis presented in this paper since it is the key to enabling the successful design of a downsized free-flying space robot.

While the benefits of downsizing a space robot are numerous, it is a challenging task with problems arising

from scaling down both the manipulator and base spacecraft. The trade-off when downsizing the manipulator is to reduce its mass and power consumption, while still maintaining a sizable dexterous workspace and high payload capacity. The preservation of the arm's dexterity is paramount since assembly tasks may involve fragile components and the connection and disconnection of joints is an arduous task; yet to be carried out in-orbit. Current technology demonstrations have not shown this high level of dexterity but instead have shown that the movement of a payload is possible (Roa et al., 2017). It is important to appreciate that the highest mass concentration is in the joints of the manipulator, and therefore, cutting down on the number of joints will lead to drastic mass reductions. However, care must be taken when removing joints to retain the manipulators dexterity; since this may induce a reduction in the DoF or manipulability. Although manipulators with less than 6 DoF can carry out a range of tasks, 6 degrees are required for full dexterity within the robots defined workspace (Gallardo-Alvarado et al., 2012).

The problems involved when downsizing the base spacecraft are due to the complex, highly non-linear, coupled dynamics of the system. Paramount to the operational success of the space robot, is its ability to remain controllable. At present, it is believed that this is the final hurdle to overcome in order for a small space robot to be deemed viable. This instability occurs due to the coupled dynamics which are a result of the micro-gravity operating environment (Chen et al., 2011). It is this phenomenon that caused the ETS-VII to fail. The coupled dynamics translate into the fact that any controlled movement of the manipulator will induce a change in the pose of the base spacecraft; a consequence of the conservation of linear and angular momentum (Zhou et al., 2019; Chen and Qin, 2017). If this induced motion is large or cannot be counteracted by the on board propulsion or attitude control subsystem (ACS), it will cause the system to become unstable and the end effector will deviate from its desired path, limiting the accuracy and precision of the system (Papadopoulos et al., 2005). This is an issue for downsized space robots since this mechanism is particularly prominent when the mass and inertia of the manipulator are not negligible in comparison to the base (Xu et al., 2016). This means that the ACS employed on the designed system must be capable of providing sufficient torque to counteract the induced motion from arm actuation. Therefore, in order to design and successfully employ a small space robot, either an ACS system that provides higher control torques at the same size must be developed, or the system must be designed in such a way that it is controllable within the limits of currently available technologies. This work therefore looks at the finding the smallest controllable system such that the benefits of downsizing are achieved with the current technologies and hardware.

The motivation behind the design of the space robot presented in this paper, is to provide a low cost, downsized alternative to the large, bespoke systems currently available. It should not be thought of as a replacement for such systems, but instead as a solution to the problems that cannot be solved with a larger system. At present, all space robots remain large and entire systems are tailored towards a single mission objective. Current small satellites show that the required technologies are available, however the issue of dynamic coupling is yet to be addressed from a hardware design viewpoint.

This paper is an expansion of the conference paper 'Design of a small space robot for on-orbit assembly missions' (Jackson et al., 2019). This conference paper focuses on the mechanical design of the manipulator. This involves the design of the actuators, including a Finite Element (FE) analysis of the drive shaft and the appropriate gearing system, with no analysis or evaluation into the chosen sizing of the links themselves. Following this, it provides a very brief conclusion that a 12U form factor is suitable for use with the proposed manipulator, based heavily on a power analysis. On the other hand, this paper advances the proposed small space robot by focusing on why the system was sized as such; providing the analysis and explanation into the optimally sized manipulator. This paper goes further by carrying out a full dynamic analysis on the operation of the base spacecraft, therefore providing information on the optimal form factor. Also included in the conference paper is the first set of design requirements which have been refined, expanded and re-presented in this paper, along with a new, in-depth mission concept covering a range of operating modes and mission scenarios.

This paper presents an innovative design approach, whereby conclusions are driven by a dynamic analysis of the system. The outcome of this is to generate simulation-based statistics and results that provide new insight into the physical implications of the dynamic coupling effect, which is yet to be covered in the literature, although its theory has been investigated extensively by researchers. To address the aforementioned gap in the literature, this paper provides an in-depth analysis of how a space robot should be sized based on various dynamic indicators, using commercial off the shelf (COTS) components. The outcome is the confirmation that a downsized space robot is a viable option for a range of on-orbit missions, given current technology readiness of COTS CubeSat components.

The paper is structured as follows: the mission concept is introduced in Section 2; any relevant background concepts are outlined in Section 3; the choice of the manipulator and base spacecraft are then presented in Sections 4 and 5, respectively; before the paper is concluded in Section 6.

2. Mission concept

This study is driven by the commercial need to develop a small, versatile and low cost space robot capable of carrying out a range of operations on-orbit. The overarching term on-orbit operations can be split into three task groups: on-orbit assembly, active servicing and passive ser-

vicing. On-orbit assembly involves the assembly of structures or components. In the context of this research, the term assembly refers to the connection of small modules and joints on structures that would otherwise be monolithic or self-deployable. Active servicing missions involve physical contact between the space robot and at least one other body, tasks include re-fueling, component repair and component replacement. Conversely, passive servicing missions involve no physical contact between the space robot and target satellite and include missions such as fly-by's and inspections. These missions could be carried out with the space robot acting as a rigid body, with no manipulator actuation. As a result the phenomenon of dynamic coupling is not present, so these missions are not considered in the context of this work. The system design presented in this paper is for small space robots, where the base spacecraft weighs less than 500 kg (Sweeting, 2018). Nevertheless, the design methodology presented can be equally applied to other larger space robots.

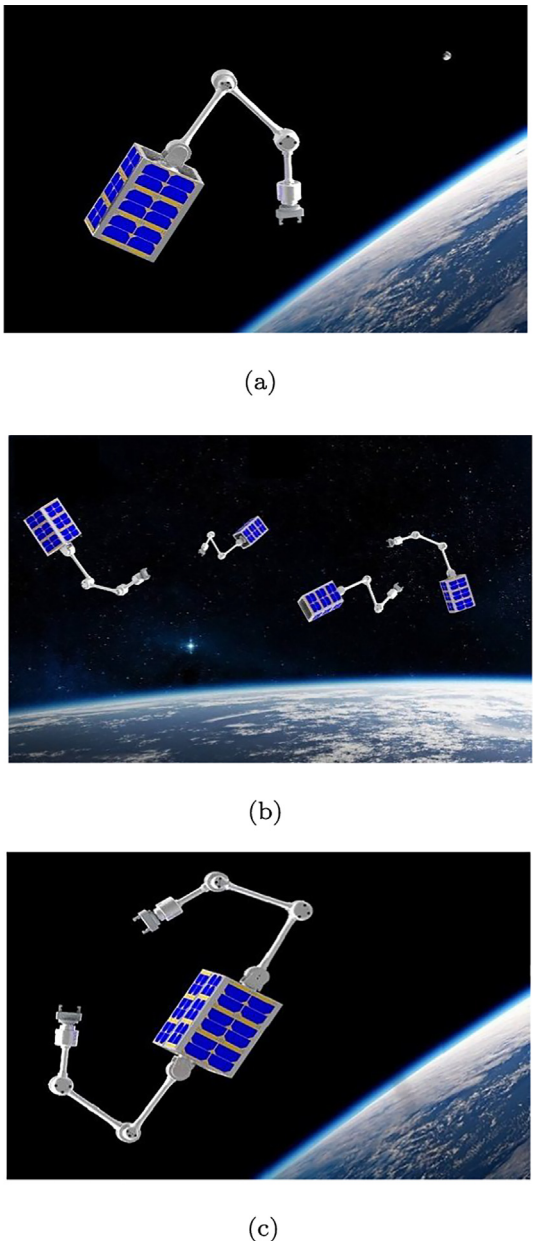

Fig. 1. Different operating scenarios using the proposed space robot (a) Single system (b) Multi-agent system (c) Dual arm system.

The system will be capable of functioning in one of the three different operating scenarios in order to facilitate the successful operation of a range of tasks. The first is a single system (Fig. 1(a)), the second scenario (Fig. 1(b)) involves a number of space robots flying in a swarm, acting as a multi-agent system. The final operating scenario (Fig. 1 (c)) is a dual arm system; increasing the spacecraft's dexterity through dual arms.

Table 1 shows a list of potential missions, the corresponding subsystem requirements and the operating scenario that is thought to be optimal to achieve each task. Here, values are derived from the attributes of the target payload in each mission. From Table 1 it is possible to derive a set of design requirements for the entire system, these are summarised in Table 2. It should be noted that this table does not encapsulate all subsystem level requirements, but those that apply in the context of this dynamic based design approach. For example, capability for intelligent perception or up-link and down-link rates, do not affect the dynamic interaction between the arm and base and are not considered at this time. It is important to highlight that the use of the dual system in the case of debris removal allows the reach of a single manipulator to be 0.5 m while still achieving the necessary 1 m for this mission scenario. While a number of different mission concepts are presented here, it should be noted that the capability of such a space robot is extensive and not limited to the missions highlighted. However, in order to undertake this design exercise it was necessary to outline a number of specific tasks, allowing a set of requirements for the space robot to be defined.

The trajectory carried out by the arm is mission dependent and will also heavily impact the performance of the spacecraft. A number of motions have been defined and assigned to each mission. In practice, one mission may include a number of motion profiles, however, this would be addressed in the path planning algorithms, which are beyond the scope of this research. The profiles used in this analysis can be seen in Table 3, with the specific joint motions given in Appendix A.

3. Background concepts

Throughout this paper the size of the base spacecraft is defined using the CubeSat standard, where satellites are made from a number of units. Units are 0.1 m × 0.1 m × 0.1 m, each of which is estimated to weigh 1.33 kg (Qiao et al., 2013).

The dynamic model of the space robot was used to investigate how changing the size of the manipulator and

Table 1
System requirements (Strobl et al., 2014; Gao et al., 2009; You, 2018; Cappelletti et al., 2018; Ellery et al., 2008; Forshaw et al., 2016).

No.	Mission tasks	Subsystem requirement	Operating scenario
1	Assemble solar arrays	Payload mass ≈ 100 g Desired reach ≈24 cm End effector accuracy ≈ ± 2 mm Able to apply force of ≈20 N End effector opening ≈1 mm	Swarm
2	Mount Antenna	Payload mass ≈80 g end effector accuracy ≈ ± 2 mm	Single system
3	Replace optics	Standard camera mass <1 kg No fumes released during process End effector accuracy ≈ ± 1 mm	Single system
4	Replace micro-propulsion system	Payload mass <5 kg Independent payload actuation End effector opening of ≈80 mm	Dual system
5	Remove broken subsystem from functioning satellite	Ability to keep base stationary 12 DoF giving high dexterity Payload mass of up to 5 kg	Dual system in swarm
6	Removal of small space debris	Payload mass ≈5 kg End effector opening of 8 cm Reach of ≈1 m	Dual system

Table 2
Design requirements.

Requirement	Description
FR_01	System will be able to independently manipulate a payload
FR_02	System will be operate in free-flying and free-floating mode
PR_01	System will be able to manipulate a payload of 5 kg
PR_02	End effector will apply forces greater than 50 N
PR_03	Manipulator will have a length of 0.5 m
PR_04	End effector will have accuracy of at least ±2 mm
PR_05	End effector opening of 80 mm
DR_01	The system will have 12 DoF
DR_02	Base spacecraft mass will not exceed 50 kg
DR_03	Manipulator will weigh less than 5 kg

FR: Functional requirement. PR: Performance. Requirements. DR: Design Requirements.

Table 3
Difference in motion profiles for each mission.

Mission	Description
1	Large motion with no effector twist to allow for the movement of large components
2	Small motion with end effector twist to mount a smaller components
3	Small precise motion, including small rotation of the end effector for joint connection
4	Large motion of the arm with end effector twist for component connection/disconnection
5	Larger motion with end effector twist for payload relocation
6	Smaller motion of the arm for minor payload relocation

form factor of the base spacecraft affects its performance. The formation of the dynamic model that represents a space robot with an 'n' DoF manipulator has been well investigated and laid out in previous literature. An in-depth explanation into the derivation used in this paper can be found in Virgili-Llop et al. (2017, 2015, 1993, 2018, 2019). While the derivation is not outlined here an overview of the required equations is given. These equations are valid based on the following assumptions:

- Each link acts as a rigid body.
- Payload capture has occurred and is modeled as an additional rigid body at the end of the manipulator.
- The spacecraft has suitable sensing capability.
- When the arm is not actuated the system will orbit with the expected characteristics of a standard rigid body.
- Arm actuation time is short so orbital effects are negligible during operation.

The equation used to calculate the general forces in the system is defined as follows:

$$\boldsymbol{\tau} = \mathbf{D}\ddot{\boldsymbol{q}} + \mathbf{C}\dot{\boldsymbol{q}}, \tag{1}$$

where

$$\mathbf{D} = \begin{bmatrix} \mathbf{D_{sc}} & \mathbf{D_{scm}} \\ \mathbf{D_{scm}^T} & \mathbf{D_m} \end{bmatrix},$$

$$\mathbf{C} = \begin{bmatrix} \mathbf{C_{sc}} & \mathbf{C_{scm}} \\ \mathbf{C_{scm}^T} & \mathbf{C_m} \end{bmatrix},$$

and

$$\boldsymbol{q} = [x \quad y \quad z \quad \alpha \quad \beta \quad \gamma \quad \theta_1 \ldots b\theta_n]^T. \tag{2}$$

Here, $\boldsymbol{q} \in \mathbb{R}^{6+n}$ is the state vector of the system, where n represents the DoF of the manipulator. In (2), the first 3 terms represent the linear position of the base (x, y, z) and the next 3 terms represent the attitude of the base (α, β, γ). These are both measured by the movement of the body fixed reference frame $(\sum b)$, with respect to the inertial reference frame $(\sum I)$. An illustration of the defined reference frames can be seen in Fig. 2. The next 'n' terms in the state vector represent the displacement of each joint of the robotic manipulator $(\theta_1 \ldots b\theta_n)$, with respect to that link's reference frame $(\sum 1, \ldots, n-1, n)$. $\dot{\boldsymbol{q}} \in \mathbb{R}^{6+n}$ are the corresponding velocities and $\ddot{\boldsymbol{q}} \in \mathbb{R}^{6+n}$, the accelerations. Each joint rotates about its own z axis. The $\mathbf{D} \in \mathbb{R}^{(6+n)\times(6+n)}$ matrix represents the inertial properties of the system where the subscript **m** relates terms to the manipulator, **sc** to the spacecraft and **scm** to the coupling between the base and manipulator. The same subscripts apply to the $\mathbf{C} \in \mathbb{R}^{(6+n)\times(6+n)}$ matrix although this time it represents the Coriolis and Centrifugal properties.

Throughout this study, the arm is controlled using a Proportional Integral Derivative (PID) controller. The desired trajectory is defined using a 5th order polynomial, constrained by the initial and final joint positions, velocities and accelerations (Seddaoui and Saaj, 2017). The starting and final velocity and acceleration were all set to zero. The initial position of the arm for each mission is the 'zero' orientation, whereby all joint displacements are set to zero, and the arm is extended, utilizing its full reach. The final positions are defined by the motions given in Table 3. It should be noted that while these motions are related to the corresponding missions, the use of the 'zero' starting position may not be employed in practice. This is an acceptable approximation, as the chosen trajectories encompass the full joint range and the systems ability to return to this 'zero' position is investigated.

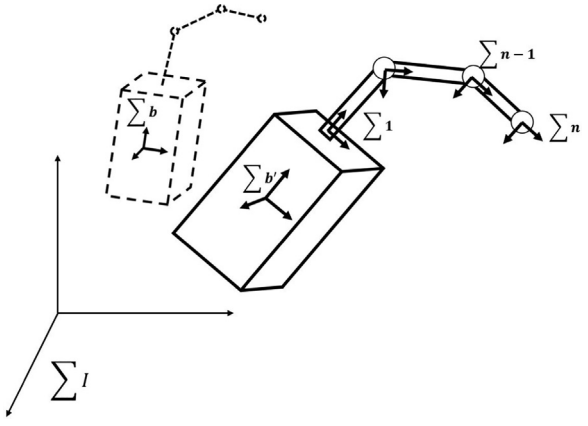

Fig. 2. Reference frames used with space robot. $\sum b$ is the body fixed reference frame whose origin is at the center of mass of the base spacecraft. $\sum I$ is the inertial reference frame, and the numbered frames refer to the different links.

The space robot can be controlled in one of two modes: with an uncontrolled base (free-floating mode) or a controlled base (free-flying mode), both are investigated in this paper. For the free-floating operating mode, no forces are applied to the base spacecraft, and if present, the ACS will be turned off. This means the first 6 terms of the control signal ($\boldsymbol{u}$) are set to 0, where $\boldsymbol{u}$ is then defined as follows:

$$\boldsymbol{u} = \begin{bmatrix} F_x & F_y & F_z & \tau_x & \tau_y & \tau_z & \tau_{(\theta_1 \ldots \theta_n)} \end{bmatrix}^T. \tag{3}$$

Here, $F_{x,y,z}$ represents the linear control forces on the base spacecraft in each of the axis, in newtons, $\tau_{x,y,z}$ represents the control torque about each axis, in newton-meters and $\tau_{(\theta_1 \ldots b\theta_n)}$, the control torque at each joint, also in newton-meters. Since $F_{x,y,z}$ and $\tau_{x,y,z}$ are set to zero in the free-floating mode, the base is free to move as a result of the dynamic coupling forces generated due to actuation of the arm. As outlined by Nenchev (2013), it is possible to plot the null reaction space of the manipulator, i.e an area in inertial space where motion of the end effector does not disturb the base. This means that even when operating in the free-floating mode, it will be possible to manipulate the arm without changing the pose of the satellite. For the free-flying operating mode, the base will be 3-axis stabilised and any forces due to arm actuation will be counteracted by the satellites ACS (Dubanchet et al., 2015). This means that the arm will always be operating off a fixed base, even if the end effector leaves the null reaction space. In this case, the first 6 terms of the control signal ($\boldsymbol{u}$) are determined using a PID controller with the linearised dynamic model and computed torque control in conjunction with further feed-forward compensation. The dynamic coupling forces are used as the feed-forward control signal, since this enables the system to pre-empt the reactive forces applied to the base. The feed-forward control signal ($\boldsymbol{F_{ffc}}$) is defined as:

$$\boldsymbol{F_{ffc}} = \begin{bmatrix} 0 & \mathbf{D_{scm}} \\ \mathbf{D_{scm}^T} & 0 \end{bmatrix} \ddot{\boldsymbol{q}} + \begin{bmatrix} 0 & \mathbf{C_{scm}} \\ \mathbf{C_{scm}^T} & 0 \end{bmatrix} \dot{\boldsymbol{q}}, \tag{4}$$

and is added to the PID control signal ($\boldsymbol{F_{PID}}$) to calculate the final control signal. It uses only the $\mathbf{D_{scm}}$ and $\mathbf{C_{scm}}$ terms in the **D** and **C** matrices since these quantify the dynamic coupling effect. The first 6 terms of the control signal ($\boldsymbol{u}$) are defined by:

$$\boldsymbol{u}_{1:6} = \boldsymbol{F_{ffc}} + \boldsymbol{F_{PID}}. \tag{5}$$

This is combined with the required joint torques and integrated into the dynamic model via the general force equation:

$$\ddot{\boldsymbol{X}} = \mathbf{D}^T(\boldsymbol{f}_c - \mathbf{C}\dot{\boldsymbol{\theta}}), \tag{6}$$

where,

$$\boldsymbol{f}_c = \begin{bmatrix} \boldsymbol{u}_{1:6} \\ \boldsymbol{u}_{arm} \end{bmatrix}. \tag{7}$$

The dynamic model was set up in Simulink using the standard block library. The parameters of the designed manipulator, including the actuator saturation limits, link lengths and link masses are all used in the model. The mass and dimensions of the base spacecraft also act as parameters to the system. Also used in the model is the max allowable speed of the arm actuators, set as 0.25 rad/s. Inputs to the model are the initial and final joint displacements and the mass and dimensions of the form factor in question. Each simulation was run over 200 time steps, and 1 control signal is received per 1 s time step.

4. Design of the robotic manipulator

The driving factors when downsizing the robotic manipulator are to minimise the total mass while maintaining end effector accuracy, overall reach and dexterity. This applies to the dynamic approach in this paper since the error is a function of base deviation, and the reach and mass affect the arms inertia, which in turn affects the dynamic coupling forces that are applied to the base spacecraft. Three variations of link length were generated and investigated. All link proposals were generated to conform with the following rules:

1. Link 0 has a length of 0 mm, due to the combination of joints 1 and 2. This maintains the dexterity of manipulator while minimising weight.
2. Link 3 is shortest since this allows for increased end effector accuracy. With the same actuator accuracy, a shorter link length will result in more accurate end effector placement.
3. Total length will match the specified reach (PR_03). A minimum of three links are needed to provide the required DoF.
4. All links will be constrained to factors of 5 cm. This ensures ease of manufacture and design as well as constraining the design space to feasible limits.

Table 4
Proposed arm configurations.

	Link 1 (m)	Link 2 (m)	Link 3 (m)	Total length (m)
1	0.2	0.2	0.1	0.5
2	0.25	0.15	0.1	0.5
3	0.3	0.15	0.05	0.5

The details of the different configurations can be seen in Table 4, while a schematic of each configuration can be found in Fig. 3.

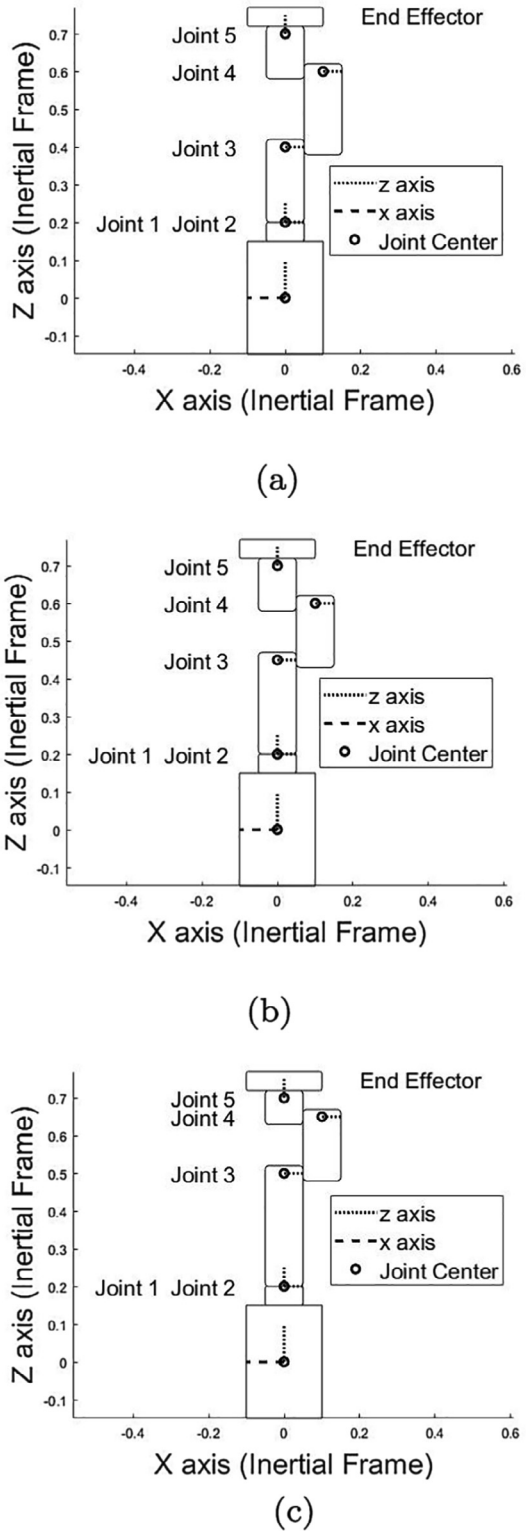

Fig. 3. Proposed arm configurations, each joint rotates about its z axis (a) Option 1 (b) Option 2 (c) Option 3.

The workspace of each different link configuration was plotted and compared (Fig. 4). The same joint limits were used across all the proposed configurations; set at $\pm 50°$. The additional reach of the end effector is not considered here since the same component will be used with each configuration. From this it can be seen that option 1 hosts the largest workspace. It is inferred that if the joint limit changes so will the workspace of the manipulator. However this change will be consistent across all options, meaning the comparison made here will still be valid.

Following this, the end effector accuracy for each different option was looked at. In accordance with the mission concept, the accuracy must be $\approx \pm 2$ mm to assemble solar arrays and mount antenna and $\approx \pm 1$ mm to replace optics. None of the other missions specify a hard accuracy constraint, hence, the error analysis was run for these three missions. The payload capacity was set to a $1\,\text{kg}, 8\,\text{cm}^3$ cube for all simulations and the base was operated in the free-flying mode (ACS employed to maintain 'zero' deviation). Error in the final position is shown in Table 5. The error given is the resolution of the vector error in the inertial reference frame. It should be pointed out that at present the error due to other hardware limitations is not included in the simulation.

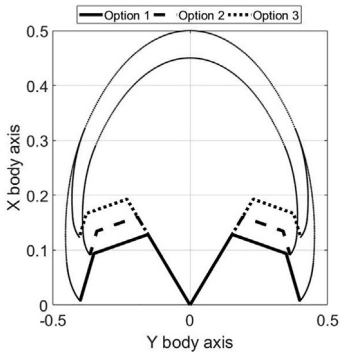

Fig. 4. Workspace area for all three configurations.

Table 5
Error in the final positioning of the end effector. Mission 1 is to assemble solar arrays. Mission 2 is to mount and antenna and mission 3 is to replace optics.

Mission	Arm configuration	Final error (mm)	Allowable error (mm)
1	1	3.32	2 mm
	2	3.09	
	3	2.78	
2	1	2.00	2 mm
	2	2.10	
	3	1.92	
3	1	0.97	1 mm
	2	1.04	
	3	0.06	

It can be seen that none of the proposed arm configurations conform with the accuracy requirement to assemble solar arrays. Further, only options 1 and 3 conform with the other mission's accuracy requirement. The lack of conformity in regards to solar array assembly is discussed later, in Section 5. Disparity in error across configurations, for the same mission, is seen as the varying link lengths affect the inertial distribution and therefore the size of the dynamic coupling components. This in turn, affects the orientation and position of the base in the inertial reference frame, which then effects the positioning of the arm, in the same frame. Errors also stem from the controller itself, although this is not considered an issue in the context of this study since the same controller was used for all scenarios. In practice the controller would be fine tuned to the specific manipulator.

From here, options 1 and 3 are further investigated to ensure requirements PR_01, PR_02 and PR_05 are also satisfied. Since the end effector selected for use (Jackson et al., 2019) has a max opening of 85 mm, it can be said that PR_05 is satisfied. It also has a payload capacity of 5 kg and a grip force of 235N, therefore, provided manipulation of this payload does not cause excessive deflection or fracture of the links, the remaining two requirements can be said to be satisfied. Deflection was checked using the static torque experienced by the links due the combination of their, and the payload's mass, modeled here as a point mass of 5 kg. The static torque (τ_s) was calculated using Eq. (8), where $\boldsymbol{r} \in \mathbb{R}^3$ is the vector distance between the links CoM and the point of interest.

$$\tau_s = \boldsymbol{r} \times \boldsymbol{F} \tag{8}$$

In this simulation the point of interest is the top of each link. The static torque will be a maximum when the manipulator is fully stretched (all $\theta = 0°$), hence this is the orientation used. The maximum occurs in this orientation since the arm is fully stretched, leading to the longest feasible torque arm. $\boldsymbol{F} \in \mathbb{R}^3$ is the force applied by the inertial distribution of the rest of the system. This is calculated using the link masses and the maximum acceleration of the actuators, defined as 0.25 rad/s, about each links z axis (Jackson et al., 2019). A tapered hollow tube was selected for the link shape due to the low mass, and high strength. The internal space also allows for the wiring to be contained. At this stage, the links are set to be manufactured from aluminum (density of $2700\,\text{kg/m}^3$).

An FE analysis on options 1 and 3 yielded the results shown in Table 6, which also shows the inputs used in the simulations. Each link was modeled as being fixed at one end with the static torque applied at the other, an image of this can be seen in Fig. 5, which also shows the shape of the links. Each simulation used the same sized tetrahedral mesh, with a varying number of nodes. The maximum stress experienced by the link was also determined during the FE analysis, and is quoted in Table 6.

Table 6
Results and inputs used in the FE analysis.

Arm config.	Link	Link mass (kg)	Static torque (N m)	Maximum Deflection (mm)	Maximum Stress (MPa)
1	1	0.054	0.232	0.00794	0.573
	2	0.054	0.100	0.00343	0.243
	3	0.027	0.034	0.00067	0.141
3	1	0.081	0.199	0.0253	0.551
	2	0.0405	0.049	0.000711	0.108
	3	0.0135	0.034	0.000098	0.115

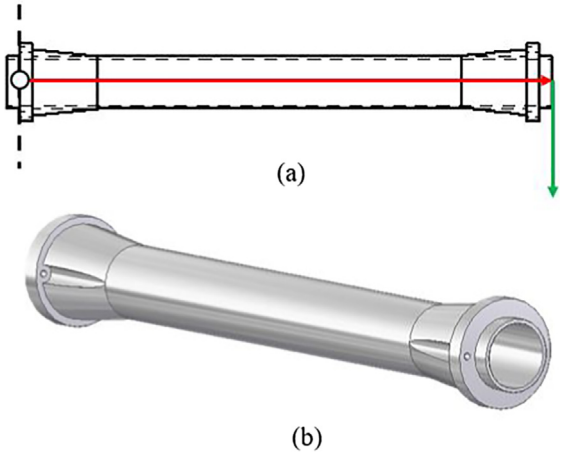

Fig. 5. (a) Engineers drawing of the link. Green arrow: force applied. Red arrow: torque arm. Black circle: axis of rotation. Black dotted line: face fixed during simulation. (b) Computer generated drawing of link. (For interpretation of the references to colour in this figure legend, the reader is referred to the web version of this article.)

This is the Von Mises stress, the simulation was run with the same parameters as the deflection analysis.

Although this is a simplification since in practice the links will not be fixed at one end, it provides a good estimate. It can be seen that all levels of deflection are very small and the stresses experienced are far from the yield stress of aluminum (UTS $\approx$ 310 MPa). From this FE analysis, it can be said that both link configurations are suitable for use, based on the reasonable assumptions made here. Although options 1 and 3 both conform with all design requirements at this stage, option 1 was selected since it hosts the largest workspace. It should again be pointed out that neither of these configurations provide low enough error to carry out the assembly mission as it is currently defined.

Fig. 6 shows the final design of the proposed manipulator, while its properties are summarised in Table 7.

5. Design of base spacecraft

Table 8 shows the subsystem requirements that apply to the downsizing of the base spacecraft. Provided the base has 6 controllable DoF, requirements FR_01 and DR_01 will be satisfied; both of which are independent of the base

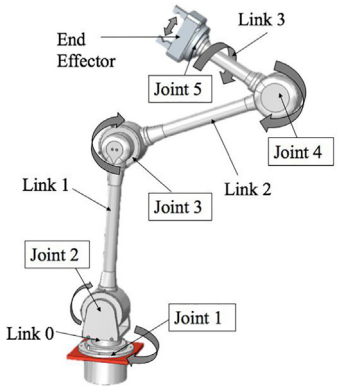

Fig. 6. Naming convention for the robotic manipulator (Jackson et al., 2019).

Table 7
Manipulator parameters.

Component	Mass (kg)	Length (m)	Range (°)
End Effector	0.9	[0; 0; 0.5]	n/a
Link 0	0	[0; 0; 0]	n/a
Link 1	0.054	[0; 0; 0.2]	n/a
Link 2	0.054	[0; 0; 0.2]	n/a
Link 3	0.027	[0; 0; 0.1]	n/a
Joint 5	0.407	n/a	±50
Joint 4	0.496	n/a	±50
Joint 3	0.496	n/a	±50
Joints 1/2	0.96	n/a	Joint 2 = ±50 Joint 1 = ±90
TOTAL	3.394		

spacecraft size. In accordance with FR_02 the system must be able to operate in the free-flying and free-floating mode (where the change is in the control signal used with the base spacecraft). In practical missions, free-floating is often not a preferred mode of operation due to unlimited workspace, non-holonomic behaviour and likelihood of dynamic singularity. Despite these limitations, it is necessary to ensure that it is a feasible mode of operation. This is due to the fact that the ACS or propulsion system may malfunction and it is imperative that this does not render the system useless. The system may also need to run in a low power or fuel mode, meaning either or both subsystems will be turned off. Specific missions also dictate reduced use of linear control thrusters to limit the extent of gas impingement on sensitive payloads; mission 3 is an example of this. In all

Table 8
Refined requirements that apply to the sizing and design of the base spacecraft. Modification of Table 2.

Requirement	Description
FR_01	System will be able to independently manipulate a payload
FR_02	System will be operate in free-flying and free-floating mode
PR_01	System will be able to manipulate a payload of 5 kg
DR_01	The system will have 12 DoF
DR_02	Base spacecraft mass will not exceed 50 kg

FR: Functional requirement. PR: Performance. Requirements. DR: Design Requirements.

of these cases, it is crucial that motion of the end effector can cause the base to change its pose, giving the system a level of control, while ensuring that the pointing requirements of the base spacecraft are satisfied.

For performance in the free-flying mode to be deemed acceptable, thus satisfying the first part of requirement FR_02, the ACS and linear propulsion system must be capable of maintaining the base spacecraft in a 'zero' deviation position. This is reliant on the subsystems operational limits and the availability of sufficient power and fuel. The ACS selected for use is the RWPo15 MicroWheel, provided by Blue Canyon Technologies (Blue Canyon Technologies, 2019). Three separate units will be mounted, capable of providing 4×10^{-3} N m of torque in any axis. This acts as the limit for the allowable control torque. This hardware was selected since it has a low operating power, small footprint, and strong flight heritage. The propulsion system selected for use is the C-POD cubesat propulsion system, a cold gas propulsion system made by VACCO, with an I_{sp} of 40 s and total fuel mass of approximately 1.244 kg. If life time is estimated to 10,000 trajectories, prior to refueling the limit on the control force is 0.00568N. This particular propulsion system was selected due to its low weight, low power draw and flight heritage.

For performance in the free-floating mode to be deemed acceptable, thus satisfying the second part of requirement FR_02, base deviation must be less than 30° (∼ 0.5 rad), about any axis. This value is derived from the cameras chosen for use with the system. The selected camera was chosen due to its flight heritage and low cost. The 60° field of view means a deviation of more than 30°, as a result of the dynamic coupling between the arm and the base will lead to loss of sight of the payload (Forshaw et al., 2016). In practice, if fitted with more than one camera, the payload may then come into view of another sensor, or, if the path planning algorithm accounts for the effect of the dynamic coupling the payload may never leave the robots field of view. However, path planning is beyond the scope of this research and is not considered here. In linear terms, this translates to a maximum deviation of 0.28 m in any direction, assuming that the payload is 0.5 m away. This is guaranteed since the payload is in contact with the manipulator throughout this study. Requirement FR_02 can therefore be broken down into the following requirements, all of which must be satisfied:

1. Free-floating mode:
   - Arm actuation must result in an angular deviation of less than 0.5 rad about any axis.
   - Arm actuation must result in linear deviation of less that 0.28 m in any axis.

2. Free-flying mode:
   - Torque required from ACS must not exceed 4×10^{-3} N m about any axis.
   - Force required from thrusters must not exceed 0.00568 N in any axis.

The same control hardware is used for all the form factors in question since the motivation of this study is to provide the smallest, operable space robot. The selection of downsized hardware keeps the required footprint, cost, mass and power demands to a minimum, allowing the smallest system possible to be designed. Requirement PR_01 will be validated by ensuring that all the previous requirements are satisfied while the manipulator is holding a payload of 5 kg. This is acceptable since it has already been proven that the arm can manipulate a payload of this mass (Jackson et al., 2019). The last requirement that applies to the sizing of the base spacecraft is DR_02. Table 9 summarises the different form factors investigated and it can be seen that all of these comply with requirement DR_02. It should be noted that the masses used here are an estimated based on the idea that 1 form factor unit weighs 1.33 kg (Qiao et al., 2013). Compliance with requirement FR_02 is done by analyzing the space robots performance in the free-floating and free-flying operation modes.

Table 9
Form Factor Properties, masses and dimensions are estimates, and will depend on the final design of the integrated system.

Form Factor	Mass (kg)	Dimensions (m) (height × width × depth)
3U	4	0.3 × 0.1 × 0.1
6U	8	0.3 × 0.2 × 0.1
12U	16	0.3 × 0.2 × 0.2
18U	23.9	0.3 × 0.3 × 0.2
24U	31.9	0.3 × 0.4 × 0.2
27U	35.9	0.3 × 0.3 × 0.3

5.1. Free-floating operation mode

Of interest in this simulation is the base deviation as a result of arm actuation. Fig. 7 shows the magnitude of the dynamic coupling forces and moments, applied to a 3U form factor, as a result of actuating the arm along an arbitrary trajectory. This graph shows the erratic nature of the reaction forces and moments. These act as a disturbance to the base and the arm and as a consequence, the required torque and force applied at each joint and to the spacecraft, display the same irregular attributes. However, due to the short time period over which the variations occur, the arm and base motion hosts a much smoother nature, shown in Fig. 8. The magnitude of this base motion, and therefore the final base position, is a function of the form factor of the base spacecraft. An illustration of this can be seen in Fig. 9. This figure shows that the base deviation is larger in the case of the 3U form factor spacecraft due to its lower inertia, compared to the 27U form factor spacecraft. The resulting increased positional error of the end effector can also be seen.

In order to assess the optimum form factor for the base spacecraft, it was necessary to determine the magnitude of the base deviation due to arm actuation, therefore validating the limits derived from requirement FR_02. The dynamic model was run for each form factor for the 6 missions and the maximum linear and attitude deviation was extracted. This is the deviation of the body fixed reference frame with respect to the inertial reference frame (Fig. 2).

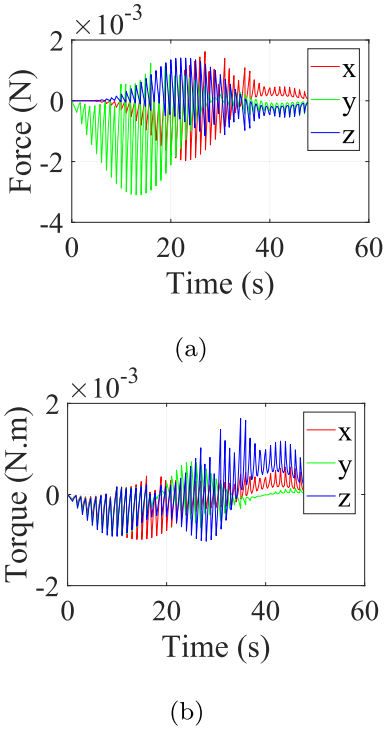

Fig. 7. Reaction forces and torques due to dynamic coupling acting on a 3U base spacecraft as a result of the arm tracking a pre-defined trajectory (a) Linear force (b) Torque.

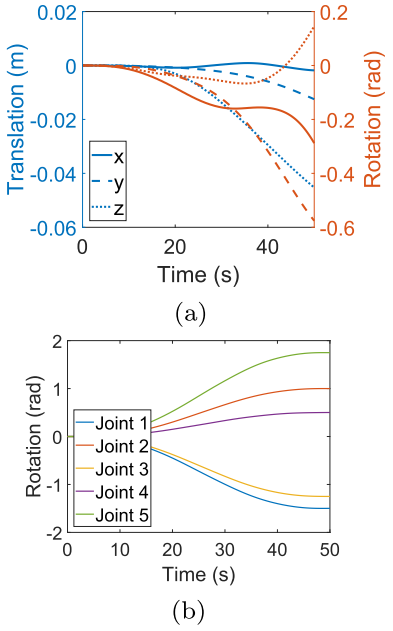

Fig. 8. Resultant motion for 3U form factor of the (a) Base spacecraft (b) Joints.

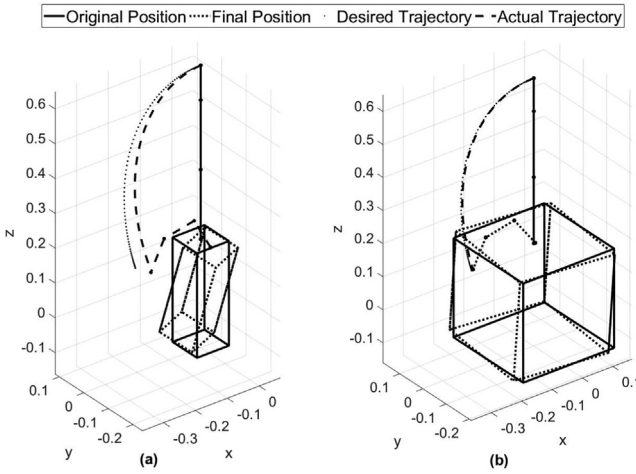

Fig. 9. Error in arm trajectory and base spacecraft deviation as a result of arm actuation for (a) 3U form factor (b) 27U form factor.

The results are shown in Fig. 10. These graphs show the modulus of the maximum deviation value for the entire trajectory. It can be seen that both the linear and rotary deviation decrease in a gradual manner with increasing form factor, as expected, due to the change in ratio of base inertia to arm inertia.

The allowable limit for attitude deviation is 0.52 rad and is represented by the line in Fig. 10(a). From this it can be seen that all missions carried out on an 18U, or larger, form factor comply with specified limit. However, it was shown in Section 4 that the chosen manipulator configuration is incapable of providing low enough error to carry out the assembly of solar arrays (mission 1). Removing this mission from the list means that a 12U form factor, with

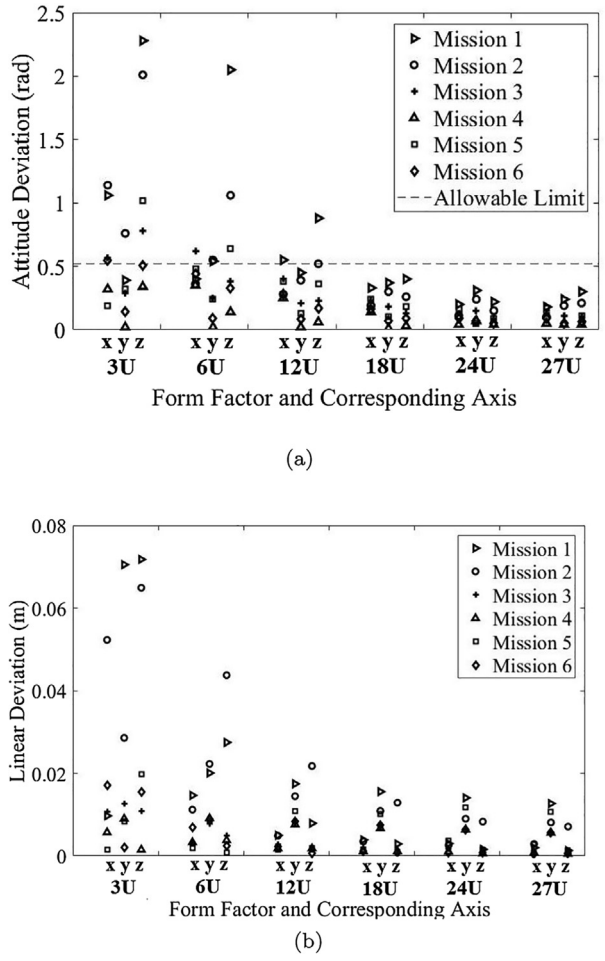

Fig. 10. Maximum base deviation for a range of form factors in the free-floating operating scenario in each of the 6 missions. (a) Attitude (b) Translation.

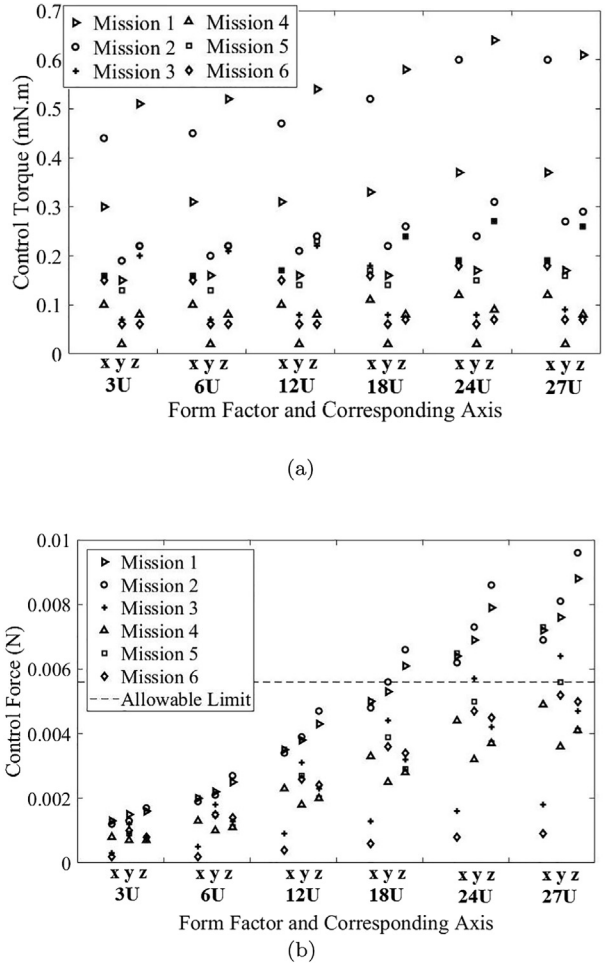

Fig. 11. Control torques and forces for a range of form factors to maintain 'zero' deviation throughout arm actuation. Base is operating in the free-flying mode. (a) Torque (b) Force.

the proposed manipulator, satisfies all the requirements thus far. The maximum allowable linear deviation in this operating mode is 0.28 m, which all the form factors are well within.

5.2. Free-flying operation mode

The simulation was run again, this time including the control signal generated by the PID controller with feed-forward compensation, as outlined in Section 3. As a result, control forces were applied to the base to maintain its pre-defined 'zero' pose. The impact of the arm's motion was investigated assuming that the base spacecraft had already been stabilized to its 'zero' position. The system was therefore, not trying to return the base state vector to a given location, but was instead aiming to maintain its state. This emulates a situation in which the payload has already been captured, and the combined system stabilised. The maximum required forces to preserve this position, can be found in Fig. 11. These forces correspond to the limits derived from requirement FR_02. This figure shows the modulus of the maximum values for the 6 mission scenarios used throughout this paper. From this it can be seen that the controller is capable of maintaining the base spacecraft's 'zero' position using very small control torques and linear forces for all form factors. It should be pointed out that for all options of form factor, across all missions, the base deviation was approximately zero.

The control torques required are all well within the pre-defined limit, and are shown to increase only very slightly with increasing form factor. The forces required to maintain the linear position of the space robot increase linearly with form factor.

The mission concepts were defined based on the manipulator starting at a 'zero' position. In order to validate this assumption, simulations were run to ensure that the system could return to this 'zero' position after each mission was complete. Such simulations were run by using the final position and velocity of the arm and the base, from the free-floating experiments, as the dynamic model inputs. A simulation was run for each of the missions and the results can be seen in Fig. 12. Excluding mission 1, it can be said that any form factor size 12U or above is capable of return-

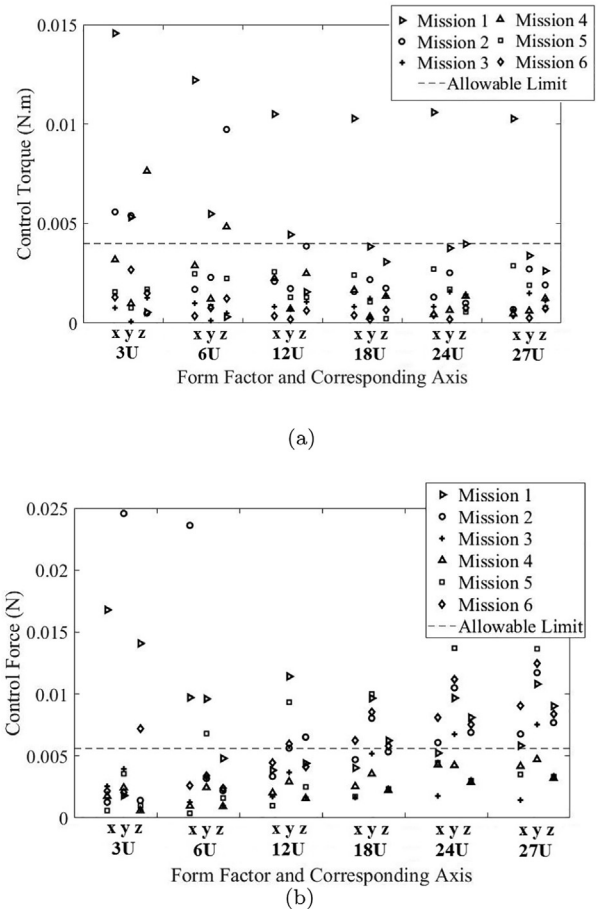

Fig. 12. Control torques and forces for a range of form factors to return the system back to 'zero' position. (a) Torque (b) Force.

ing to 'zero' position within the ACS limits. However, the propulsion limit is below the control forces needed, for all missions and form factors.

5.3. Discussion

The simulation results are used to prove compliance of each sized space robot with requirement FR_02. For the free-floating analysis, it can be seen that any form factor above 18U exhibits allowable attitude deviation. The 12U form factor is suitable if the assembly mission, defined in this paper, is disregarded. In the case of the 12U form factor, the space robot proposed is suggested for use with only on-orbit servicing missions; with the recommendation that a larger system be used in the context of assembly missions. In regards to the linear deviation, all form factors are within the limits given by the pointing requirements of the satellite. It can be seen that as form factor increases the deviation falls. This is due to the increase in spacecraft inertia reducing the effect of the dynamic coupling forces.

Analysis of the results from the free-flying simulations show that in all cases a 'zero' position can be maintained to an acceptable level of accuracy. The forces required for linear position maintenance increase linearly with increasing form factor. This is due to the holonomic nature of the reaction effect. It is seen that, even with the exclusion of the assembly mission, only a form factor sized 3U, 6U or 12U are within the limits prescribed by the chosen propulsion system. Varying the form factor has very little overall effect on the control torques required to maintain the satellites attitude. This is because the forces required to correct the same deviation increase with the mass of the base spacecraft. However, as highlighted in the free-floating simulation, with increasing form factor the deviation needing to be corrected falls; these changes therefore act to cancel each other out. Due to the nature with which both of these factors vary, it is expected that this relationship extends beyond the 27U form factor. When comparing the required control torque values to that available from the ACS (0.04 N m) it can be seen that the subsystem is able to provide sufficient torque for all the form factors for all missions investigated.

The last section of analysis looks at the control forces and torques required to return the system to its 'zero' position upon mission completion. Again, excluding the assembly mission it can be said that any form factor sized 12U or larger can be maneuvered to this position within the ACS limits. However, even with the exclusion of mission 1, the control forces required are well above the limit set by the propulsion system. While this is undesirable it does not render the system unusable as this was a guide based on average fuel consumption, not the maximum force that the propulsion system can exert. Instead, this increased demand will translate to a higher fuel consumption per return mission. Mission designers should, therefore, recall that the system operates at lower dynamic requirements if starting from the 'zero' position.

This analysis concludes that the smallest possible space robot to conform with all the design requirements outlined in Section 2 should have a 12U form factor base spacecraft. At this size, the spacecraft can perform the specified tasks while maintaining the pointing requirements set by the on-board sensors.

5.4. Fuel and power

The dynamic analysis in Section 5.2, incorporated a fuel analysis. It showed that for a set number of trajectories excessive fuel was not required to stabilize the base spacecraft. However, it was shown that returning the arm to its 'zero' position, required more fuel. While this appeared to exceed the allowable level, this is not a physical limit of the hardware. Instead it means more fuel is required for these maneuvers, lowering the overall life time of the satellite. The fuel required for station keeping and orbit insertion is not considered in this paper. These will be factored into the overarching mission for launch and maintenance of the space robot as opposed to the in-orbit missions addressed in this study.

Following the dynamic analysis, it was necessary to ensure that the recommended form factor was also capable

Table 10
Power demands of subsystems. Demand is split into operational time i.e when the arm is being actuated and station keeping i.e, arm is not actuated. Duty cycle of arm is not included as this is the total power required for the actuation. This includes both the mission and return to 'zero' position.

Subsystem		Station Keeping			Operational		
		Power (W)	Duty Cycle (%)	Total (W)	Power (W)	Duty Cycle (%)	Total (W)
Payload	Arm	0	0	0	0.00542	n/a	0.00542
Comms	UHF	1.9	10	0.19	0.19	0	0
	VHF	0.15	90	0.135	0.15	10	0.015
Control	ACS	1	90	0.9	3	10	0.3
	Prop	1	90	0.9	3	10	0.3
	Sensors	5.6	40	2.24	5.6	10	0.56
Thermal	Heaters	1.5	90	1.35	1.5	10	0.15
Power	Power system electronics	0.05	90	0.045	0.05	10	0.005
Subtotal				5.76			1.33542
Total							7.095

of generating enough power to run the necessary subsystems. The estimated levels of power consumption were determined by researching COTS components suitable for use with the proposed system, and looking at the duty cycle of each subsystem. Choices were made based on flight histories and specific system requirements (Wertz and Larson, 1999). It should be noted that a passive thermal control system was chosen for use with this system in order to keep power consumption to a minimum. The hot and cold equilibrium temperatures for the 12U form factor were calculated and it was deduced that a layer of multi-layer insulation (MLI), placed between the solar panels and body of the base spacecraft, would be sufficient to maintain its internal temperature within the required range; provided the on-board batteries are insulated further. The power budget was calculated assuming that the system carries out two trajectories per orbit, constituting one mission and a return to the 'zero' position. This constitutes a 10% duty cycle assuming the satellite is in a 400 km orbit. The power demands of the different subsystems are shown in Table 10. The power generated from the body mounted solar panels was calculated using the method outlined by Dahbi et al. (2015). The assumption is made that the panels are to be mounted on the 4 largest sides of the base spacecraft, giving an overall panel surface area of 0.072 m^2. Body mounted panels were chosen, since deployable panels would limit the space in which the system could operate, as well as reducing its versatility and maneuverability. Based on these assumptions, the average available power is 8.02 W throughout the orbit. Provided the power regulation subsystem is designed correctly along with the selection of suitably sized batteries, the 12U form factor is capable of supplying sufficient power to complete one mission per orbit.

5.5. Structure

In line with the previous analysis, the base spacecraft chosen is a 12U platform with body mounted solar panels, dimensioned 0.3 m × 0.2 m × 0.2 m. The structure consists of four upright struts onto which an outer shell is mounted, a layer of Multi Layer Insulation (MLI) then sits between this shell and the solar panels, which form the exterior surface of the satellite. This set up creates a hollow structure into which the required subsystems can be stacked.

Table 11
Subsystem mass.

Component	Mass (kg)
Base Structure	2.7
Arm	3.4
Communications	0.3
Control	7.2
Thermal	1
Power	0.9
TOTAL	15.5

The top face provides an interface between the robotic arm and the base spacecraft, and consists of a mounting point compatible with joints 1/2; the bottom face is left bare to fix the antenna. The system will be equipped with a micro strip patch antenna due to its small size, simple nature and low cost (Kakoyiannis and Constantinou, 2008). This antenna is also easy to integrate, allowing high levels of flexibility based on the data and up/down link requirements of specific missions.

The subsystems required for successful operation of the base spacecraft and their respective masses can be found in Table 11, which highlights that at present the base spacecraft weighs 15.5 kg, which conforms with requirement DR_02, the entire base must weigh less than 50 kg.

6. Conclusion

Discussed in this paper is a dynamic based approach for designing the smallest sized space robot capable of carrying out a range of on-orbit operations. This unique design approach was taken since current state-of-the-art CubeSat

technologies mean the issue of the dynamic coupling is the last hurdle to overcome prior to the successful deployment of small space robots. The in-depth dynamic analysis conducted at system level leads to the conclusion that a 12U form factor is the smallest sized system capable of hosting the compact 5 DoF manipulator. This is based on a number of mission concepts and design requirements, all of which are outlined in this paper. At this size, the system will be capable of successfully operating in the free-flying or free-floating mode. The system design was driven by non-mission specific requirements meaning it can be used in conjunction with a range of servicing missions. While the assembly mission defined in this paper cannot be achieved, it might be possible to re-define such a mission to conform with the specification of the proposed manipulator. The results presented in this paper support the hypothesis that the deployment of a downsized space robot is technically feasible, and that present COTS based space qualified ACS hardware for CubeSats and manipulators is capable of supporting such a system.

As it stands the design does not provide the ability for two identical systems to dock and operate in a conjoined manner with dual arms, as suggested in the mission concepts. To address this use-driven need, further work is being carried out into the design of a docking plate. This will allow the system to carry out more complex tasks on heavier target spacecraft. A more robust control system that will account for the environmental perturbations, is also under development and will be published separately. This is because it will be suitable for use in conjunction not only with this space robot but also on other, larger systems.

Acknowledgments

The authors would like to thank Surrey Satellite Technolgy Ltd. and the Engineering and Physical Sciences Research Council for funding this research.

Appendix A. Joint Motion

See Table A.12.

Table A.12
Final joint positions for each of the missions analysed. Note that the starting position for all joints across all trajectories is zero degrees.

Mission	Joint angle (°)				
	1	2	3	4	5
1	50	50	50	50	0
2	0	45	0	45	90
3	0	0	30	45	45
4	30	−45	−30	−45	90
5	45	45	0	−45	−45
6	30	−30	0	−30	0

References

Blue Canyon Technologies, 2019. 'Reaction wheels data sheet'. <https://storage.googleapis.com/blue-canyon-tech-news/1/2019/10/BCT_Data-Sheet_Components_ReactionWheels_F2.pdf> (Date Accessed: 16/12/2019).

Boumans, R., Heemskerk, C., 1998. The european robotic arm for the international space station. Robot. Auton. Syst. 23 (1–2), 17–27.

Bowman, L.M., Belvin, W.K., Komendera, E.E., Dorsey, J.T., Doggett, B.R., 2018. In-space assembly application and techonolgy for NASA's future science observatory and platform missions. In: 'Proc. SPIE Astronomical Telescopes and Instrumentation', Austin, Texas, 12–14 Jun, pp. 690–708.

Cappelletti, C., Battistini, S., Graziani, F., 2018. Small launch platforms for micro-satellites. Adv. Space Res. 62 (12), 3298–3304.

Chen, H., Li, D., Guo, S., 2011. Analyzing dynamic coupling effect resulted by space operations with recursive formulation. In: 'Proc. IEEE 5th International Conference on Robotics, Automation and Mechatronics (RAM)', Qingdao, China, 17–19 Sept, pp. 332–337.

Chen, X., Qin, S., 2017. Kinematic modeling for a class of free-floating space robot. IEEE Access 5, 12389–12403.

Chung, S.-J., Adams, D., Saenz-Otero, A., Kong, E., Miller, D.W., Leisawitz, D., Lorenzini, E., Sell, S., 2006. SPHERES tethered formatin flight testbed: advancements in enabling NASA's SPECS mission. In: 'Proc. SPIE Astronomical Telescopes and Instrumentation', 6268, Orlando, Florida, USA, 24 – 31 May.

Dahbi, S., Aziz, A., Zouggar, S., Benazzi, N., Zahboune, H., Elhfyani, M., 2015. Design and sizing of electrical power source for a nanosatellite using photovoltaic cells. In: 'Proc. 3rd IEEE International Renewable Sustainable Energy Conference', Isreal, 10–13 Dec, pp. 1–6.

Debus, T.J., Dougherty, S.P., 2009. Overview and performance of the front-end robotics enabling near-term demonstration (FREND) robotic arm. In: 'Proc. AIAA Infotech @Aerospace Conference', Seattle, Washington, 6–9 Apr, p. 1870.

Doggett, W.R., Dorsey, J.T., Jones, T.C., King, B., 2014. Development of a tendon-actuated lightweight in-space MANipulator (TALISMAN). In: 'Proc. 42nd Aerospace Mechanisms Symposium', Vol. 405, NASA Goddard Space Flight Center, 14–16 May, pp. 405–420.

Dubanchet, V., Saussie, D., Alazard, D., Berard, C., Peuvedic, C.L., 2015. Modeling and control of a space robot for active debris removal. CEAS Space J. 7 (2), 203–218.

Dubowsky, S., Papadopoulos, E., 1993. The kinematics, dynamics and control of a free-flying and free-floating space robotic system. IEEE Trans. Robot. Autom. 9 (5), 531–543.

Ellery, A., Kreisel, J., Sommer, B., 2008. The case for robotic on-orbit servicing of spacecraft: spacecraft reliability is a myth. Acta Astronaut. 63 (5), 632–648.

Flores-Abad, A., Ma, O., Pham, K., Ulrich, S., 2014. A review of space robotics technologies for on-orbit servicing. Prog. Aerosp. Sci. 68, 1–26.

Forshaw, J.L., Aglietti, G.S., Navarathinam, N., Kadhem, H., Salmon, T., Pisseloup, A., Joffre, E., Chabot, T., Retat, I., Axthelm, R., Barraclough, S., Ratcliffe, A., Bernal, C., Chaumette, F., Pollini, A., Steyn, W.H., 2016. Removedebris: an in-orbit active debris removal demonstration mission. Acta Astronaut. 127, 448–463.

Friend, R.B., 2008. Orbital express program summary and mission overview. In: 'Proc. SPIE 6958, Sensors and Systems for Space Applications II', Vol. 65803, Orlando, Florida, USA, 15 April.

Gallardo-Alvarado, J., Alici, G., Rodriguez-Castro, R., 2012. A novel three degrees of freedom partially decoupled robot with linear actuators. Robotica 30, 467–475.

Gao, S., Clark, K., Zackrisson, J., Shiroma, W.A., Akagi, J.M., Maynard, K., Garner, P., Boccia, L., Amendola, G., Massa, G., Underwood, C., Brenchley, M., Pointer, M., Sweeting, M.N., 2009. 'Antennas for modern small satellites', IEEE Antennas Propag. Magaz., pp. 40–56.

Jackson, L., Saaj, C., Seddaoui, A., Whiting, C., Eckersley, S., Ferris, M., 2019. Design of a small space robot for on-orbit assembly missions. In:

'Proc. 5th International Conference on Mechatronics and Robotics Engineering', Rome, Italy, 17 – 18 Feb, pp. 107 – 112.

Kakoyiannis, C.G., Constantinou, P., 2008. A compact microstip antenna with tapered peripheral slits for CubeSat RF payloads at 436MHz: iniaturization techniques, design and numerical results. In: 'Proc. IEEE International Workshop on Satellite and Space Communications', Toulouse, France, 1–3 Oct, pp. 255–259.

Liu, X.-F., Li, H.-Q., Chen, Y.-J., Cai, G.-P., Wang, X., 2015. Dynamics and control of capture of a floating rigid body by a spacecraft robotic arm. Multibody Syst. Dynam. 33, 315–332.

Miller, D.W., Mohan, S., Budinoff, J., 2008. Assembly of a large modular optical telescope (ALMOST). In: 'Proc. SPIE 7010, Space Telescopes and Instrumentation 2008: Optical, Infrared and millimeter', 70102H, Marseille, France, 12 July.

Mulder, T.A., 2008. Orbital express autonomous rendezvous and capture flight operations. part 2 of 2. In: 'Proc. AIAA/AAS Astrodynamics Specialist Conference and Exhibit', Honolulu, Hawaii, 18–21 Aug, p. 6768.

Nanjangud, A., Blacker, P., Bandyopadhyay, S., Gao, Y., 2018. Robotics and AI-enabled on-orbit operations with future generation of small satellites. Proc. IEEE 106 (3), 429–439.

Nenchev, D.N., 2013. Reaction null space of a multibody system with applications in robotics. Mech. Sci. 4, 97–112.

Oda, M., 1999. Space robot experiments on NASDA's ETS-VII satellite - preliminary overview of the experiment results. In: 'IEEE International Conference on Robotics and Automation', Vol. 1–4, Detroit, MI, USA, 10–15 May, pp. 1390–1395.

Papadopoulos, E., Tortopidis, I., Nanos, K., 2005. Smooth planning for free-floating space robots using polynomials. In: Proc. 2005 International Conference on Robotics and Automation', Barcelona, Spain, 18 – 22 April, pp. 4272–4277.

Penin, L.F., Matsumoto, K., Wakabayashi, S., 2000. Force reflection for ground control of space robots. IEEE Robot. Autom. Magaz. 7, 50–63.

Qiao, L., Rizos, C., Dempster, A.G., 2013. Analysis and comparison of a cubesat lifetime. In: 'Proc. 13th Australian Space Conference', Sydney, Australia, 30 Sep – 2 Oct, pp. 246–249.

R. Sullivan, B., Kelm, B., Roesler, G., Henshaw, C., 2015. Robotic satellite servicer concept: On-demand capabilities in geo. In: 'Proc. AIAA Space Conference', Pasadena, California, 31 Aug–2 Sep.

Reed, B.B., Smith, R.C., Naasz, B., Pellegrino, J., Bacon, C., 2016. The restore-L servicing mission. In: 'Proc. AIAA Space Forum', Long Beach, California, 13–16 Sep.

Reintsema, D., Sommer, B., Wolf, T., Theater, J., Radthke, A., Sommer, J., Naumann, W., Rank, P., 2011. DEOS - the in-flight techonolgy demonstration of germans robotics approach to dispose of malfunctioned satellites. In: 'Proc. ESA Workshop on Advanced Space Technologies for Robotics and Automation'., ESTEC Noordwijk, The Netherlands, 12–14 April.

Rembala, R., Ower, C., 2009. Robotic assembly and maintenance of future space stations based on the iss mission operations experience. Acta Astronaut. 65, 912–920.

Roa, M., Nottensteiner, K., Wedler, A., Grunwald, G., 2017. Robotic technologies for in-space assembly operations. In: 'Proc. ESA 14th Symposium on Advanced Space Technologies In Robotics and Automation (ASTRA)', Leiden, The Netherlands, 20–22 Jun, pp. 1–8.

Sallaberger, C., 1997. Canadian space robotic activities. Acta Astronaut. 41 (4), 239–246.

Seddaoui, A., Saaj, C.M., 2017. Optimised collision-free trajectory and controller design for robotic manipulators. In: 'Proc. 14th Symposium on Advanced Space Technologies in Robotics and Automation', Leiden, The Netherlands, 20–22 Jun.

Seddaoui, A., Saaj, C.M., 2018. H infinity controller for a controlled floating robotic spacecraft. In: 'Proc. 14th International Symposium on Artificial Intelligence, Robotics and Automation in Space (i-SAIRAS)', Madrid, Spain, 4–6 Jun.

Seddaoui, A., Saaj, C.M., 2019. The controlled floating motion of space robots using a nonlinear H_∞ controller. AIAA J. Guid., Control Dynam. 42 (8).

Strobl, G.F.X., Ebel, L., Fuhrmann, D., Guter, W., Kern, R., Khorenko, V., Kstler, W., Meusel, M., 2014. Development of lightweight space solar cells with 30% efficiency at end of life. In: 'Proc. IEEE 40th Photovoltaic Specialist Conference', Denver, CO, USA, 8–13 Jun.

Sweeting, M.N., 2018. Modern small satellites - changing the economics of space. In: 'Proccedings of the IEEE', Vol. 106, pp. 343–361.

Virgili-Llop, J., Drew II, J.V., Romano, R.Z.M., 2017. Laboratory experiments of resident space object capture by a spacecraft-manipulator system. Aerosp. Sci. Technol. 71, 530–545.

Wenberg, D., Hardy, A., Lai, T., Wellins, C., Kang, J., 2018. Advancing on-orbit assembly with ISAR. In: 'Proc. 32nd Annual AIAA/USU Conference on Small Satellites', Utah, USA, 4–9 Aug, pp. 1–8.

Wenberg, D.L., Keegan, B.P., Lange, M.E., Hanlon, E.A.S., Kang, J.S., 2016. RSat flight qualification and test results for manipulable robotic appendages installed on 3u cubeSat platform. In: 'Proc. Small Satellite Conference', Logan, Utah, USA, 8–13 Aug, pp. 1–9.

Wertz, J.R., Larson, W.J., 1999. Space Mission Analysis and Design, third ed. Microcosm Press, ISBN: 978-1-881883-10-4.

Xu, W., Peng, J., Liang, B., Mu, Z., 2016. Hybrid modeling and analysis method for dynamic coupling of space robots. IEEE Trans. Aerosp. Electron. Syst. 52 (1), 85–98.

You, Z., 2018. Micropropulsion. Butterworth-Heinemann, Micro and Nano Technologies, ISBN 978-0-12-812672-1.

Zhou, Y., Luo, J., Wang, M., 2019. Dynamic coupling analysis of multi-arm space robot. Acta Astronaut. 160, 583–593.